

Northumbria Research Link

Citation: Jackson, John and Jannetta, Adrian (2006) Legacy data and cosmological constraints from the angular-size/redshift relation for ultracompact radio sources. *Journal of Cosmology and Astroparticle Physics*, 11. pp. 1-17. ISSN 1475-7508

Published by: IOP Publishing

URL: <http://dx.doi.org/10.1088/1475-7516/2006/11/002> <<http://dx.doi.org/10.1088/1475-7516/2006/11/002>>

This version was downloaded from Northumbria Research Link:
<https://nrl.northumbria.ac.uk/id/eprint/1394/>

Northumbria University has developed Northumbria Research Link (NRL) to enable users to access the University's research output. Copyright © and moral rights for items on NRL are retained by the individual author(s) and/or other copyright owners. Single copies of full items can be reproduced, displayed or performed, and given to third parties in any format or medium for personal research or study, educational, or not-for-profit purposes without prior permission or charge, provided the authors, title and full bibliographic details are given, as well as a hyperlink and/or URL to the original metadata page. The content must not be changed in any way. Full items must not be sold commercially in any format or medium without formal permission of the copyright holder. The full policy is available online: <http://nrl.northumbria.ac.uk/policies.html>

This document may differ from the final, published version of the research and has been made available online in accordance with publisher policies. To read and/or cite from the published version of the research, please visit the publisher's website (a subscription may be required.)



**Northumbria
University**
NEWCASTLE



UniversityLibrary

Legacy data and cosmological constraints from the angular-size/redshift relation for ultra-compact radio sources

J C Jackson and A L Jannetta^{†‡}

[†] Division of Mathematics and Statistics, School of Informatics, Northumbria University, Ellison Place, Newcastle NE1 8ST, UK

Abstract.

We have re-examined an ancient VLBI survey of ultra-compact radio sources at 2.29 GHz, which gave fringe amplitudes for 917 such objects with total flux density $\gtrsim 0.5$ Jy. A number of cosmological investigations based upon this survey have been published in recent years. We have updated the sample with respect to both redshift and radio information, and now have full data for 613 objects, significantly larger than the number (337) used in earlier investigations. The corresponding angular-size/redshift diagram gives $\Omega_m = 0.25 + 0.04/-0.03$, $\Omega_\Lambda = 0.97 + 0.09/-0.13$ and $K = 0.22 + 0.07/-0.10$ (68% confidence limits). In combination with supernova data, and a simple-minded approach to CMB data based upon the angular size of the acoustic horizon, our best figures are $\Omega_m = 0.304 + 0.024/-0.023$, $\Omega_\Lambda = 0.693 + 0.034/-0.035$ and $K = -0.003 + 0.021/-0.019$. We have examined a simple model of vacuum energy, based upon a scalar potential $V(\phi) = \omega_C^2 \phi^2/2$, to test the possibility that the vacuum is dynamical; whereas the data favour a value $\omega_C = 0$, they are compatible with values in excess of the Hubble rate.

1. Introduction

The angular-size/redshift relationship is in principle a simple cosmological test, which has yet to play a noted part in the development of observational cosmology. Endeavours in this field have generally concentrated upon classical double radio sources as putative standard measuring rods, angular size being defined by core-lobe or lobe-lobe separation. Early results were problematical, showing angular sizes which diminish more rapidly with increasing redshift z than would be allowed by any plausible cosmological model. This behaviour is believed to be an evolutionary effect, brought about by interaction with an evolving extra-galactic medium (Legg 1970; Miley 1971; Barthel and Miley 1988; Singal 1988), or a selection effect, due to an inverse correlation between linear size and radio power (Jackson 1973; Richter 1973; Masson 1980; Nilsson *et al* 1993). There have been several attempts to disentangle the latter effects from proper cosmological ones (Daly 1994; Buchalter *et al* 1998). Daly (1994) introduces a model of lobe propagation

[‡] To whom correspondence should be addressed (john.jackson@unn.ac.uk)

which allows intrinsic size to be estimated from other source parameters; Buchalter *et al* (1998) select Fanaroff-Riley Type II sources (Fanaroff and Riley 1974) with $z > 0.3$ as the basis of their work, in part because their morphology allows an unambiguous definition of angular size, and also allow for a linear-size/redshift correlation of the sort discussed above; such measures bring the angular-size/redshift diagram for extended sources into concordance with acceptable Friedmann cosmological models, but not with sufficient precision to allow definitive statements about cosmological parameters.

More promising candidates in this context are ultra-compact radio sources, with milliarcsecond angular sizes measured by very-long-baseline interferometry (VLBI) (Kellermann 1993; Gurvits 1994). Gurvits work was based upon a large VLBI 2.29 GHz survey undertaken by Preston *et al* (1985) (hereafter referred to as P85). The latter was designed to establish a comprehensive full-sky list of ultra-compact radio sources; 1398 candidates were selected from existing surveys, on the basis of total flux density at 2.7 GHz. Selection criteria were complicated, but the candidate list is believed for example to be 97% complete to a limit of 1.0 Jy for sources with spectral index $\alpha \geq -0.5$, which comprise about 80% of the list; further details are given in the original reference. These sources were then observed in a series of VLBI experiments at 2.29 GHz; compact structure was detected in 917 cases, and the corresponding correlated flux density S_c (fringe amplitude) recorded, plus the total flux density S_t if this was measured at the same time (531 out of the 917 cases). As angular size is defined by fringe visibility S_c/S_t (Thompson *et al* 1986), the number of potential candidates for an investigation based upon P85 is thus appears to be 531. In relation to these P85 give 269 redshifts; Gurvits (1994) added further redshifts from Véron-Cetty and Véron (1991), to give a sample of 337 objects in all. Gurvits gave plausible reasons for ignoring sources with $z < 0.5$, and using just the high-redshift data (258 objects) found marginal support for a low-density Friedman cosmological model, but considered only those with vacuum energy density parameter $\Omega_\Lambda = 0$. Using exactly the same data set (kindly supplied by Dr. Gurvits), Jackson and Dodgson (1997, submitted 3/05/96) extended this work to the full density-parameter plane, and concluded that the best values are $\Omega_m = 0.2$ and $\Omega_\Lambda = 0.8$, if the Universe is spatially flat, later refined to $\Omega_m = 0.24 + 0.09 / - 0.07$ (95% confidence limits) (Jackson 2004).

The latter work develops an astrophysical model, according to which the underlying population consists of compact symmetric objects (Wilkinson *et al* 1994), comprising central low-luminosity cores straddled by two mini-lobes. Ultra-compact objects are identified as cases in which the lobes are moving relativistically and are close to the line of sight, when Dóppler boosting allows just that component which is moving towards the observer to be observed; the interferometric angular sizes upon which this work is based correspond to the said components. As z increases a larger Dóppler factor is required; it turns out that latter approximately cancels the cosmological redshift, so that the observed component is seen in its rest frame. This model, coupled with the fact that the central engines which power these sources are reasonably standard objects (black holes with masses close to $1.5 \times 10^{10} M_\odot$), gives a plausible account of their behaviour as

standard measuring rods, and of why those with $z < 0.5$ should be ignored. Those having $z \geq 0.5$ are the ultra-compact analogues (and perhaps the precursors) of Fanaroff-Riley Type II sources, and there are parallels between this work and that of Buchalter *et al* (1998). This is a slightly oversimplified precis of the account given in Jackson (2004), to which the reader is referred for further details.

We have taken a fresh look at the P85 catalogue, and updated the latter with respect to both redshift and radio information. Details of the new data set are given in Section 2. Section 2 also discusses the acoustic horizon and its linear size; coupled with accurate measures of the location of the first peak in angular spectrum of the cosmic microwave background (CMB) radiation (Balbi *et al* 2000; de Bernardis *et al* 2000; Hanany *et al* 2000, Hinshaw *et al* 2003), these allow the WMAP results to be interpreted in a simple and transparent fashion, which does not need the full machinery of CMBFAST (Seljak and Zaldarriaga 1996), that is if particular figures for Hubble's constant and baryon content are accepted. Cosmological results are presented in Section 3, for the new data alone and in combination with the most recent supernova observations (Riess *et al* 2004; Astier *et al* 2006), mainly as marginalized confidence regions in the Ω_m - Ω_Λ plane. Section 4 considers the evolution of vacuum energy in the light of the new data.

Although we believe that the results to be presented here are of intrinsic interest, a large part of our motivation in undertaking this work is to enhance further the credibility of milliarcsecond radio-sources as standard measuring rods. In this context it should be noted that their first application to the Ω_m - Ω_Λ problem (Jackson and Dodgson 1997) was blind, in the sense that it gave answers close to the concordance model at a time when Type Ia supernovae were giving $\Omega_m \sim 1$ (Perlmutter *et al* 1997). This situation did not change until the advent of Schmidt *et al* (1998), Riess *et al* (1998) and Perlmutter *et al* (1999).

2. Data

Of the 1398 sources in the P85 catalogue, 917 have definite measures of correlated flux density (the rest have upper limits), and 531 have both total and correlated flux densities. We have consulted the NASA/IPAC Extragalactic Database (NED), and find 957, 723 and 456 redshifts for the respective sub-samples (end of August 2005). Thus we have redshifts and visibilities for 456 sources; formally 8 of these have visibility > 1 and were discarded; the remaining 448 comprise our gold standard sub-sample. There are 386 sources for which a correlated flux density is listed but no total flux density ($531+386=917$); we have attempted to update this sub-sample, by searching for convenient listings in the literature which are roughly contemporaneous with P85 and at a frequency not too far removed from 2.29 GHz. With respect to southern hemisphere sources, we find that the Parkes catalogue PKSCAT90 (Parkes Catalogue 1990) serves this purpose very well. The latter gives total flux densities at 2.7 GHz, which we have extrapolated to 2.29 GHz using the spectral indices given in P85 (in the few cases where α is not listed we have used a value of zero). This procedure

gives 256 new values of S_t , for which we have 174 redshifts; formally 9 of these have visibility > 1 and were discarded; the remaining 165 sources comprise our silver standard sub-sample, which we expect to be of lower quality than the gold. We have checked the validity of this approach by considering the overlap: Figure 1 is a plot of the total flux density so extrapolated against that listed in P85, for all sources (346) for which we have both; the two figures are well correlated, with a correlation coefficient of 0.854. With respect to northern hemisphere sources, we have examined the NRAO/VLA Sky Survey (NVSS) (Condon *et al* 1998), which gives S_t at 1.4 GHz, but find that this data set (our bronze sub-sample) is less useful, being too far removed in frequency and epoch. The sample used here will comprise our gold plus silver sub-samples, amounting to 613 objects out of a possible 917, with a range $z = 0.0035$ to $z = 3.787$.

Preston *et al* (1985) selected their list of 1398 VLBI candidates mainly from an earlier version of the Parkes survey (PKSCAT85, see Parkes Catalogue 1990), and from the NRAO-Bonn survey (Kühr *et al* 1981); it would have been useful for this investigation if the corresponding flux densities had been included in P85, but this was not the case. Almost all of those sources in Kühr *et al* (1981) were re-measured at 2290 GHz by Preston *et al* (1985).

Regarding the acoustic horizon, there are several publications which give similar analytical formulae for its linear size l_{AcH} (Hu and Sugiyama 1995; Mukhanov 2004). Writing that given by Hu and Sugiyama (1995) in terms of quantities which are all evaluated at recombination of the photon-baryon plasma, we find

$$l_{\text{AcH}} = \frac{1}{\sqrt{3}} \frac{C}{A} \ln \left(\frac{A\sqrt{1+X_R} + \sqrt{A^2+1}}{A\sqrt{X_R} + 1} \right) \quad (1)$$

where

$$A = \left(\frac{3\rho_b}{4\rho_\gamma} \right)_r^{1/2} = \left(\frac{3\rho_c}{4\rho_\gamma} \frac{\Omega_b h^2}{1+z_r} \right)_0^{1/2} \quad (2)$$

$$X_R = \left(\frac{\rho_m}{\rho_R} \right)_r^{-1} = \left(\frac{\rho_c}{\rho_R} \frac{\Omega_m h^2}{1+z_r} \right)_0^{-1} \quad (3)$$

$$C = 2c \left(\frac{8\pi G \rho_m}{3} \right)_r^{-1/2} = 2c (\Omega_m H_0^2)^{-1/2} (1+z_r)^{-3/2}. \quad (4)$$

Here ρ_c is the critical density corresponding to a particular value of Hubble's constant $H_0 = 100h \text{ km sec}^{-1} \text{ Mpc}^{-1}$; subscripts b and m refer to baryons and baryons+cold dark matter, and γ and R to CMB photons and photons+neutrinos, respectively; a subscript r refers to values at recombination, and zero to current values. Equation (1) is exact only in the case of flat cosmologies, but in practice flatness will hold to a high degree of accuracy for any realistic model, over the interval between the big bang and recombination. It is exact also only in the case of instantaneous recombination at some redshift z_r , which is unrealistic; in reality recombination starts at a redshift of about 1200 and is complete at about 800. For this reason equation (1) underestimates the

size of the acoustic horizon, because it does not allow for those charged baryons which recombine in the period immediately preceding z_r , and curtails acoustic propagation too early (Mukhanov 2004). We have allowed for this by devising a semi-empirical two-parameter fitting formula, which increases l_{AcH} by a factor $\alpha(\Omega_b, h)$, and reduces ρ_R by a fixed factor β ; the latter is effective because it allows more time for acoustic propagation to take place. Taking $z_r = 1088$ (Hinshaw *et al* 2003) and three massless neutrinos, we find that the following values are appropriate § :

$$\alpha = 1.2047 + 1.008(\Omega_b - 0.04) + 0.1178(h - 0.7) \quad (5)$$

$$\beta = 0.602. \quad (6)$$

Comparison with numerical results from CMBFAST show that with these modifications equation (1) is accurate to better than 0.4% over the ranges $0.03 \leq \Omega_b \leq 0.05$, $0.65 \leq h \leq 0.75$ and $0.2 \leq \Omega_m \leq 0.5$, and to better than 0.6% if the latter range is increased to $0.2 \leq \Omega_m \leq 1.0$. We convert l_{AcH} into an angular scale using the correct angular-diameter distance $d_A(z)$, which need not correspond to a spatially flat model. As an example, Figure 2 shows the multipole index l_{peak} corresponding to the first Döppler peak in the CMB angular spectrum as a function of Ω_m , according to equation (1), in the case of spatial flatness, $\Omega_\Lambda = 1 - \Omega_m$.

For Type Ia supernovae (SNe Ia) we have used a composite data set comprising objects from Riess *et al* (2004) (the gold sample) and Astier *et al* (2006) (The Supernova Legacy Survey, SNLS). Each of these samples includes a low- z subset ($z \leq 0.125$, 68 and 44 objects respectively); the two low- z subsets are not identical, but have 21 objects in common. Our composite data set comprises the full gold sample from Riess *et al* (2004) (157 objects) plus 71 high- z objects from Astier *et al* (2006) (Table 9 of their paper); to make sure that no objects were counted twice, we do not include the SNLS low- z subset in our composite sample. However, before assembling the latter there is a matching problem to be considered, discussed below.

The distance indicator listed in both Riess *et al* (2004) and Astier *et al* (2006) is distance modulus μ_B ; to bring the two samples into conformity we find that it is necessary reduce the gold subset distance moduli by 0.14 magnitudes. This figure was determined by fitting the equation

$$\mu_B = 5 \log_{10}(z) + C \quad (7)$$

first to the low- z gold subset, and then to the low- z SNLS one; the best values are $C = 43.37$ and $C = 43.23$ respectively. We choose the low- z subsets for this purpose (rather than the full ones), because they overlap, and because the outcome does not depend upon a choice of cosmological parameters.

The probable reasons for this offset are outlined below. Astier *et al* (2006) list a rest-frame maximum-luminosity magnitude m_B^* for each supernova, from which they

§ Including z_r dependence the equation is: $\alpha = 1.1991 + 7.0 \times 10^{-4}(z_r - 1080) + [1.020 - 1.5 \times 10^{-3}(z_r - 1080)](\Omega_b - 0.04) + [0.121 - 4.0 \times 10^{-4}(z_r - 1080)](h - 0.7)$

derive a corresponding magnitude m_B corrected for brighter-slower and brighter-bluer correlations, which reduce the dispersion in magnitude by a factor of about 2 (see for example Guy *et al* 2005 and the references given there). The magnitudes so corrected were used in a Hubble diagram to derive a best-fitting absolute magnitude $M = -19.31 + 5 \log_{10}(h/0.7)$, which was subtracted from the corrected magnitudes to give the listed distance moduli. The latter thus depend on the choice of Hubble's constant; Astier *et al* (2006) adopt $h = 0.7$ as their fiducial value. Although knowledge of these parameters is not essential to the determination of cosmological parameters, which depend only upon magnitude differences, they are nevertheless useful adjuncts. Riess *et al* (2004) follow a similar procedure, but do not mention values of H_0 and M explicitly (see the discussion in their Appendix A); there is no reason to suppose that the implicit values are the same as those used by Astier *et al* (2006). Having reduced the gold values by 0.14 magnitudes before combining the two lists, it is a matter of taste whether we use distance moduli or corrected magnitudes as working variables; we prefer the latter, and have reconstructed a table of same by adding -19.31 to each μ_B in our composite list. In what follows we marginalize over the absolute magnitude M , rather than treat it as a fixed parameter.

3. Cosmological parameters

With respect to the milliarcsecond radio-sources, our procedure follows that given in Jackson (2004). Of the 613 sources mentioned in Section 2, 468 have $z > 0.5$, with $0.501 \leq z \leq 3.787$. These are placed in appropriate redshift bins, and the mean redshift and a suitably defined characteristic angular size θ relating to each bin comprise our data points; our working numbers are logs of θ . As in Jackson (2004), we find that the best compromise (between many bins containing few objects and a small number containing many) is to have 6 bins, which conveniently is a divisor of 468 to give 78 objects in each. This number of bins is comfortably larger than the number of parameters to be determined, and the correspondingly large number of objects within in each accurately determines the characteristic angular size. To derive confidence regions, we give each point equal weight, and define a corresponding standard deviation: $\sigma^2 = \text{residual sum-of-squares}/(n-p)$, relative to the best-fitting curve defined by Ω_m , Ω_Λ and d , where $n = 6$ is the number of points and $p = 3$ is the number of fitted parameters; here d a characteristic linear size associated with the source population. The definition of 'characteristic' in this context is discussed at length in Jackson (2004), where it is shown that there is a clear inverse correlation between linear size and absolute radio luminosity. In a flux-limited sample those sources with large redshift are intrinsically the most powerful, which means that the corresponding size distribution is biased towards intrinsically smaller objects; this introduces a weak bias towards open universes, if characteristic angular size within each bin is taken to be the simple mean. As a countermeasure the characteristic angular size is defined as a median biased towards the lower end of the size distribution, namely the boundary between the bottom third

and the top two thirds of the latter. With 78 objects in each bin the boundary is defined by the 26th point; in fact we take the mean of points 16 to 36 (i.e. 26 ± 10) as a somewhat smoother measure than the 26th point alone, but this range is not critical. With this definition we find best-fitting values $\Omega_m = 0.22$, $\Omega_\Lambda = 1.06$ and $d = 7.75h^{-1}$ kpc, and a standard deviation $\sigma = 0.0074$ in $\log \theta$, i.e. 1.7% in θ . To show that these figures are robust with respect to binning, we have repeated the calculation for 15 bin sizes, from 13 bins of 36 objects to 6 bins of 78 objects, in steps of 3 objects, retaining the maximum redshift of 3.787 in each case and using the largest number of bins compatible with having no objects with $z < 0.5$. The outcome is $\Omega_m = 0.24 \pm 0.04$, $\Omega_\Lambda = 1.01 \pm 0.07$, and curvature parameter $K = 0.25 \pm 0.04$ (68% confidence limits). These figures are consistent with those derived from a confidence region, discussed below. The question of robustness with respect to the definition of characteristic angular size will be considered at the end of this section.

Rather than rely too heavily upon a particular binning, we have produced points corresponding to bin sizes of 76, 77 and 78 objects, for which the respective standard deviations in $\log \theta$ are $\sigma = 0.0125$, 0.0031 and 0.0074; our working points are a composite of these three cases. We do not add smaller bins, because this generally means discarding valuable data close to $z = 0.5$. The resulting data points are shown in Table 1; the standard deviation is now $\sigma = 0.00603$. The red plots in Figure 3 shows 68% and 95% confidence regions in the Ω_m - Ω_Λ plane, marginalized over the nuisance parameter d ; 1-dimensional projections give $\Omega_m = 0.25 + 0.04 / - 0.03$, $\Omega_\Lambda = 0.97 + 0.09 / - 0.13$ and $K = 0.22 + 0.07 / - 0.10$ (68% confidence limits).

Table 1. Data points for the angular-size/redshift relationship; θ is in milliarcseconds.

z	θ
0.6153	1.4624
0.8580	1.2801
1.1527	1.1599
1.4200	1.1448
1.8288	1.1760
2.5923	1.2374

With respect to the acoustic horizon, the key observational point is the position of the first peak in the CMB angular spectrum, now located precisely at multipole moment $l_{\text{peak}} = 220.1 \pm 0.8$ (Hinshaw *et al* 2003). We must first specify values of H_0 and $\Omega_b h^2$, and will adopt the Wilkinson Anisotropy Microwave Probe (WMAP) values $H_0 = 72 \pm 5$ km sec $^{-1}$ Mpc $^{-1}$ and $\Omega_b h^2 = 0.024 \pm 0.001$ (68% confidence limits) (Spergel *et al* 2003). Strictly speaking we should not use values which derive from the angular spectrum, but these figures are well supported by independent observations, Cepheid variables in the case of H_0 (Freedman *et al* 2001; Altavilla *et al* 2004; Riess *et al* 2005), and nucleosynthesis considerations for $\Omega_b h^2$ (D’Oderico *et al* 2001; Kirkman *et al* 2003; Pettini and Bowen 2001). If equation (1) is used to calculate the size of the

acoustic horizon the biggest source of uncertainty arises from the uncertainty in Hubble's constant; l_{AcH} changes by $\pm 2.9\%$ as H_0 changes over the above error range, whereas the corresponding figure for $\Omega_b h^2$ is $\pm 0.28\%$. Thus our procedure is to fix $\Omega_b h^2$ at 0.024, set $l_{\text{AcH}} = d_A(z_r) \times \pi/220$, and regard equation (1) as giving h as a function of Ω_m and Ω_Λ . Equation (1) is solved to give h at each point in the Ω_m - Ω_Λ plane, where $d_A(z_r)$ is the corresponding angular-diameter distance; we then define values $\chi^2 = [(h - 0.72)/0.05]^2$, which with 1 degree of freedom gives the appropriate confidence region. Note that the error in l_{peak} is quite negligible in this context. The continuous blue lines in Figure 3 define 95% confidence limits; the fit is exact along the dashed blue line, which has slope -1.255 and intersects the flat (magenta dotted) line at $\Omega_m = 0.271$. The slight curvature in the contours at the low-density end of the diagram is because radiation still makes a significant contribution to the total density at z_r : $(\rho_R/\rho_m)_{z_r} = 0.45$ when $\Omega_m = 0.1$.

The green plots in Figure 3 show 68% and 95% confidence regions for $157 + 71 = 228$ SNe Ia, marginalized over absolute magnitude M . In weighting each point we have followed exactly the scheme given in Astier *et al* (2006); each magnitude is assigned a variance $\sigma_p^2 + \sigma_{\text{int}}^2$, where σ_p is the listed photometric error, and σ_{int} is a fixed error attributed to intrinsic variations, which is chosen to give a minimum value of χ^2 equal to the expected figure 225. We find $\sigma_{\text{int}} = 0.105$ for our composite sample; we have checked the corresponding figure for the full (nearby plus distant) SNLS sample, and find $\sigma_{\text{int}} = 0.131$, which coincides with the value given in Astier *et al* (2006).

A summary of best-fitting cosmological parameters is given in Tables 2 and 3, for the three basic samples separately and in various combinations.

Table 2. Best-fitting cosmological parameters, 95% confidence limits; MAS=milliarcsecond radio-sources, AcH=acoustic horizon, SN=Type Ia supernovae.

Sample	Ω_m	Ω_Λ	K
MAS	$0.25 + 0.09 / - 0.06$	$0.97 + 0.15 / - 0.34$	$0.22 + 0.11 / - 0.26$
MAS+AcH	$0.31 + 0.08 / - 0.06$	$0.69 + 0.09 / - 0.11$	$-0.01 + 0.04 / - 0.05$
SN	$0.39 + 0.18 / - 0.21$	$0.86 + 0.31 / - 0.38$	$0.25 + 0.47 / - 0.57$
SN+AcH	$0.30 + 0.07 / - 0.06$	$0.69 + 0.08 / - 0.09$	$-0.01 + 0.04 / - 0.04$
MAS+SN	$0.31 + 0.05 / - 0.04$	$0.76 + 0.12 / - 0.15$	$0.07 + 0.12 / - 0.14$
MAS+SN+AcH	$0.30 + 0.05 / - 0.04$	$0.69 + 0.06 / - 0.07$	$0.00 + 0.04 / - 0.04$

Figure 4 is an alternative presentation of the same information, in which the coordinates have been transformed to the deceleration parameter $q_0 = \Omega_m/2 - \Omega_\Lambda$ and curvature parameter $K = \Omega_m - \Omega_\Lambda - 1$. The best figures for q_0 are -0.55 ± 0.09 (95%) and ± 0.05 (68%). Figure 4 is clearly compatible with the conclusion that we are living in a spatially flat Universe with accelerating expansion.

The outstanding question relates to robustness of the MAS figures with respect to definition of characteristic angular size. If we use simple means instead of biased medians, 68% figures for MAS alone become $\Omega_m = 0.28 + 0.06 / - 0.04$, $\Omega_\Lambda =$

Table 3. Best-fitting cosmological parameters, 68% confidence limits; MAS=milliarcsecond radio-sources, AcH=acoustic horizon, SN=Type Ia supernovae.

Sample	Ω_m	Ω_Λ	K
MAS	$0.249 + 0.041 / - 0.031$	$0.969 + 0.089 / - 0.135$	$0.218 + 0.066 / - 0.103$
MAS+AcH	$0.308 + 0.038 / - 0.033$	$0.687 + 0.047 / - 0.054$	$-0.005 + 0.022 / - 0.024$
SN	$0.389 + 0.096 / - 0.104$	$0.856 + 0.165 / - 0.183$	$0.245 + 0.249 / - 0.277$
SN+AcH	$0.300 + 0.033 / - 0.032$	$0.694 + 0.040 / - 0.042$	$-0.006 + 0.020 / - 0.020$
MAS+SN	$0.309 + 0.024 / - 0.024$	$0.763 + 0.065 / - 0.071$	$0.072 + 0.063 / - 0.070$
MAS+SN+AcH	$0.304 + 0.024 / - 0.023$	$0.693 + 0.034 / - 0.035$	$-0.003 + 0.021 / - 0.019$

$0.74 + 0.18 / - 0.30$ and $K = 0.02 + 0.14 / - 0.25$, which represent a significant shift towards open universes, but not to an extent which alters the overall qualitative picture. This shift illustrates the point made in the first paragraph of this section, and is precisely the effect found in Jackson (2004). With respect to composite data sets the shift is of virtually no consequence, figures for MAS+SN+AcH becoming $\Omega_m = 0.29 + 0.03 / - 0.02$, $\Omega_\Lambda = 0.70 + 0.03 / - 0.04$ and $K = -0.01 + 0.02 / - 0.02$.

4. Evolution

We do not attempt here to map out the evolution of vacuum energy with cosmic time t . The consensus is that large volumes of high-quality data will be needed to do this in an unambiguous way (Aldering 2005; Mosoni *et al* 2006), an order of magnitude greater than those available currently. The vacuum equation-of-state is characterised by the ratio of vacuum pressure to vacuum energy density, denoted by $w(z)$. Simple functional forms have been used to model evolution, for example $w = w_0 + w_1 z$ (Cooray and Huterer 1999) and $w = w_0 + w_1 z / (1 + z)$ (Linder 2003); however, Maor *et al* (2002) have shown by means of simulated data and counter-example that such parametrizations can produce very misleading results. If w is assumed to be constant then the best-fitting value does not necessarily coincide with the time-averaged value. In general there is a propensity to produce apparently well-fitting functions $w(z)$ which are distinctly more negative than they should be, in some cases significantly less than -1 ; the latter are generally regarded as unphysical (see also Maor *et al* 2001; Linder 2004; Jónsson *et al* 2004; Bassett *et al* 2004, Jassal *et al* 2006). There are also non-parametric approaches (Chiba and Nakamura 2000; Daly and Djorgovski 2003, 2004; Gerke and Efstathiou 2002; Huterer and Turner 1999, 2001; Huterer and Starkman 2003; Wang and Freese 2006)

As an alternative to the simple functional forms $w(z)$ mentioned above, we shall use a proper physical model of dynamical vacuum energy, based upon the simple potential

$$V(\phi) = \omega_C^2 \phi^2 / 2 \tag{8}$$

where ω_C is the Compton frequency of the corresponding boson. If it turns out that the data favour a value $\omega_C > 0$, we shall take this as evidence that the Universe is governed

by a scalar vacuum energy which is diminishing with time in a reasonably smooth way, rather than a cosmological constant, and not as support for the particular potential (8). In other words we are using the latter to test the hypothesis that the rate-of-change of vacuum energy is zero. In what follows we shall assume that the Universe is spatially flat, and that the true cosmological constant is strictly zero. Corresponding to the said potential, we have scalar density

$$\rho_\phi = (\dot{\phi}^2 + \omega_C^2 \phi^2)/2 \quad (9)$$

and pressure

$$p_\phi = (\dot{\phi}^2 - \omega_C^2 \phi^2)/2. \quad (10)$$

The relevant Friedmann equation for the scale factor $R(t)$ is

$$\ddot{R} = -\frac{4\pi}{3}G(\rho_\phi + 3p_\phi + \rho_m + 2\rho_R)R = -\frac{4\pi}{3}G(2\dot{\phi}^2 - \omega_C^2 \phi^2 + \rho_m + 2\rho_R)R \quad (11)$$

and the scalar field is governed by the equation

$$\ddot{\phi} + 3H\dot{\phi} + \omega_C^2 \phi = 0 \quad (12)$$

where $H = \dot{R}/R$ is the instantaneous value of Hubble's 'constant'.

To solve the system of equations (11) to (12), it is convenient to introduce dimensionless variables $x = R/R_0$, $y = \dot{x} = \dot{R}/R_0$, and

$$u = \left(\frac{4\pi G}{3}\right)^{1/2} \phi \quad v = \dot{u} = \left(\frac{4\pi G}{3}\right)^{1/2} \dot{\phi} \quad (13)$$

where the dot is now the derivative with respect $H_0 t$, in other words our unit of time is the Hubble time. Equations (11) to (12) are then re-cast in the form of an autonomous non-linear dynamical system:

$$\begin{aligned} \dot{u} &= v & \dot{v} &= -3yv/x - \omega_C^2 u \\ \dot{x} &= y & \dot{y} &= -(2v^2 - \omega_C^2 u^2) - \frac{1}{2}\Omega_m/x^2 - \Omega_R/x^3. \end{aligned} \quad (14)$$

Here ω_C is ω_C/H_0 in the old units (rather than introduce a new symbol we trust that context will dictate the appropriate form) and $\Omega_R = 8.023 \times 10^{-5}$, corresponding to $h = 0.72$. In terms of the new variables the angular-diameter distance is

$$d_A(z) = (1+z)^{-1} \frac{c}{H_0} \int_{t(z)}^{t_0} \frac{dt}{x(t)}. \quad (15)$$

By definition initial conditions (at $t = t_0$) are $x(t_0) = 1$ and $y(t_0) = 1$; those relating to u and v are in part determined in part by a specified value of the scalar density parameter $\Omega_\phi = 8\pi G\rho_\phi(t_0)/3H_0^2$, which using equations (9) and (13) becomes

$$\Omega_\phi = \omega_C^2 u(t_0)^2 + v(t_0)^2. \quad (16)$$

However, equation (12) is second order, and we must specify initial values $u(t_0)$ and $v(t_0) = \dot{u}(t_0)$ to give a unique solution, or equivalently current values of the scalar

density *and* pressure. We need to find an extra condition which fixes $u(t_0)$ and $v(t_0)$ unambiguously. To this end, we note that when $z \gtrsim 3$ we expect matter or radiation to be dominant, and $R(t) \propto t^n$, with $n = 2/3$ or $1/2$ respectively; equation (12) then becomes

$$\ddot{\phi} + \frac{3n}{t}\dot{\phi} + \omega_{\text{C}}^2\phi = 0. \quad (17)$$

Equation (17) has a regular singular point at $t = 0$, and has a two-parameter series solution, for example

$$\phi = A[1 - (\omega_{\text{C}}t)^2/6 + \dots] + \frac{B}{t}[1 - (\omega_{\text{C}}t)^2/2 + \dots] \quad (18)$$

when $n = 2/3$, and

$$\phi = A[1 - (\omega_{\text{C}}t)^2/5 + \dots] + \frac{B}{t^{1/2}}[1 - (\omega_{\text{C}}t)^2/3 + \dots] \quad (19)$$

when $n = 1/2$. The problem is that as we integrate backwards ($t < t_0$) the last term in equations (18) or (19) grows rapidly, and the corresponding vacuum energy can become dynamically dominant at critical cosmological epochs, particularly nucleosynthesis, recombination and galaxy formation. This must not be allowed to happen, and the singular component must be eliminated (Ratra and Peebles 1988). The problem is not peculiar to the particular potential (8), but is encountered whenever we use equation (12) with an explicit potential as a model of vacuum energy; in earlier work the problem was avoided by setting initial conditions at $t = 0$: $\dot{\phi}(0) = 0$ and $\phi(0)$ fine-tuned to give the desired current conditions, as in Jackson (1998), Jackson and Dodgson (1998) and Weller and Albrecht (2002). There is a possible degeneracy here, in that strictly speaking there is an allowable range of non-zero values of $|\dot{\phi}(0)| \ll \omega_{\text{C}}|\phi(0)|$; however, the constraints imposed by the above-mentioned astrophysical constraints are severe, and within the allowable range the results to be presented here are not noticeably dependent on the value of $|\dot{\phi}(0)|$. In the present context we find the above-mentioned approach somewhat cumbersome, and have adopted an alternative means of achieving the same ends, as follows.

We are almost certain that the expansion is accelerating, which in this context means that ϕ is close to its slow-roll value and is falling slowly towards the minimum in $V(\phi)$ at $\phi = 0$; during this phase we expect $\dot{\phi}$ to be given by

$$\dot{\phi} = -\frac{\omega_{\text{C}}^2\phi}{3H} \quad (20)$$

which as an initial condition on v would be

$$v(t_0) = -\omega_{\text{C}}^2u(t_0)/3. \quad (21)$$

Equations (16) and (21) together give

$$u(t_0) = \left(\frac{\Omega_{\phi}}{\omega_{\text{C}}^2 + \omega_{\text{C}}^4/9} \right)^{1/2}. \quad (22)$$

We have tried expressions (21) and (22) as starting values, and find them to be wanting. Instead we must retain a degree of freedom, and use

$$v(t_0) = -\omega_C^2 u(t_0)/\gamma \quad (23)$$

and

$$u(t_0) = \left(\frac{\Omega_\phi}{\omega_C^2 + \omega_C^4/\gamma^2} \right)^{1/2}. \quad (24)$$

The procedure is to integrate back to a suitably high fixed redshift z_f (depending on the application, for example $z_f = z_r = 1088$ to determine $d_A(z_r)$), and to find $\Omega_m(z_f)$ as a function of the variable γ . The correct value of γ is the one which maximizes $\Omega_m(\gamma, z_f)$. As an indication of the necessity of this undertaking, we quote figures for a model with current values $\Omega_m = 0.3$, $\Omega_\phi = 0.7$; with $\omega_C = 0$ we find $\Omega_m(\gamma, 10) = 0.9956$, the balance comprising scalar energy and radiation; with $\omega_C = 1$ we find $\Omega_m(3, 10) = 0.1140$, whereas the optimization procedure gives $\Omega_m(3.59, 10) = 0.9952$. In other words the slow-roll value $\gamma = 3$ gives a universe in which the scalar component becomes increasingly dominant as we move to earlier epochs, whereas for the correct value $\gamma = 3.59$ the opposite is the case.

Figure 5 shows 68% and 95% confidence regions in the ω_C - Ω_ϕ plane, to be discussed below.

5. Conclusions

In isolation, none of the techniques currently used to constrain cosmological parameters give precise numerical answers; at best we get answers to profound qualitative questions, relating particularly to acceleration and deceleration. It is only in combination that such techniques give meaningful numerical results. Nevertheless, we believe that our figures relating to milliarcsecond radio-sources are the most accurate single-technique ones to date, fully justifying the expectations expressed in the last paragraph of the Introduction; those relating to the joint samples MAS+Ach, SN+AcH and MAS+SN+Ach (Tables 2 and 3) are close to the best currently available (see for example Tonry *et al* 2003; Riess *et al* 2004; Astier *et al* 2006). Figure 5 shows that there is no evidence here for dynamical vacuum energy, in that the data prefer the value $\omega_C = 0$. However, the data are compatible with a current rate-of-change corresponding to $\omega_C = 1.34$ times the Hubble rate, which is thus faster than the latter and must be regarded as rapid. If the vacuum energy really is constant, the best we will ever do is to place limits on its variation, which is a potential dilemma for physics, because the smallest variation would suggest something like a scalar model, whereas true constancy would imply something more fundamental.

Figures 6 and 7 are graphical summaries of the data used in this investigation. The dashed blue curve is for a model with $\Omega_m = 0.304$, $\Omega_\Lambda = 0.693$. Mock radio sources were generated from supernovae using the angular-diameter distances defined by each

apparent magnitude and a fixed absolute magnitude $M = -19.28 + 5 \log_{10}(h/0.7)$, and a fixed linear size $d = 6.839h^{-1}$ pc; M and d are the best-fitting values for the samples SN and MAS respectively, when Ω_m and Ω_Λ are fixed at the above values. Mock supernovae were generated from radio sources in similar fashion. The mock radio source corresponding to the acoustic horizon was generated using d , and an angular diameter distance defined by its observed angular size and the value of l_{AcH} given by equations (1) to (4), with $h = 0.72$, $\Omega_b h^2 = 0.024$ and $\Omega_m = 0.304$. With these definitions the data points reflect the observational spread.

Postscript. As this paper was about to be submitted the WMAP three year results became available (Spergel *et al* 2006; Hinshaw *et al* 2006). We have had a quick look at the new data, to assess their impact on the figures presented above. According to the scheme adopted above we should use the new best-fitting flat Λ CDM values $h = 0.73 \pm 0.03$, $\Omega_b h^2 = 0.0223$ and $l_{\text{peak}} = 220.7$. The main effect of these changes is to move the AcH region in Figure 3 slightly to the left, so that the intersection with the flat line, previously at $\Omega_m = 0.271$, is now at $\Omega_m = 0.240$. This is in line with the WMAP three year flat Λ CDM values, alone and in combination with a number of other astronomical data sets (Spergel *et al* 2006); the exceptions are WMAP+supernovae (the gold subset of Riess *et al* (2004)) and WMAP+weak lensing data, which continue to favour somewhat higher values. Our new figures are summarized in Table 4; with the exception of the curvature parameter K , these are virtually the same as those in Table 3; the new values of K indicate a marginally open Universe; the corresponding error bars are smaller, because the blue region in Figure 3 is now narrower, but the conclusion $K < 0$ is not yet statistically significant.

Table 4. Best-fitting cosmological parameters, 68% confidence limits, taking into account the WMAP three year results; MAS=milliarcsecond radio-sources, AcH=acoustic horizon, SN=Type Ia supernovae.

Sample	Ω_m	Ω_Λ	K
MAS+AcH	$0.311 + 0.037 / - 0.034$	$0.673 + 0.046 / - 0.050$	$-0.016 + 0.017 / - 0.017$
SN+AcH	$0.297 + 0.033 / - 0.031$	$0.690 + 0.039 / - 0.042$	$-0.013 + 0.012 / - 0.013$
MAS+SN+AcH	$0.303 + 0.025 / - 0.022$	$0.684 + 0.030 / - 0.033$	$-0.013 + 0.012 / - 0.012$

Acknowledgements

This research has made use of the NASA/IPAC Extragalactic Database (NED) which is operated by the Jet Propulsion Laboratory, California Institute of Technology, under contract with the National Aeronautics and Space Administration.

References

- Aldering G, 2005 *New Astron. Reviews* **49** 346
- Astier *et al* , 2006 *Astron. Astrophys.* **447** 31
- Altavilla G *et al* , 2004 *Mon. Not. R. Astron. Soc.* **349** 1344
- Balbi A *et al* , 2000 *Astrophys. J.* **545** L1
- Barthel P D and Miley G K, 1988 *Nature* **333** 319
- Bassett B A, Corasaniti P S and Kunz M, 2004 *Astrophys. J.* **617** L1
- Buchalter A, Helfand D J, Becker R H and White R L, 1998 *Astrophys. J.* **494** 503
- Chiba T and Nakamura T, 2000 *Phys. Rev.* **D62** 121301
- Condon J J, Cotton W D, Greisen E W, Yin Q F, Perley R A, Taylor G B and Broderick J J, 1998 *Astronom. J.* **115** 1693 (<http://www.cv.nrao.edu/nvss/>) (<http://www.mrao.cam.ac.uk/surveys/nrao/NVSS/NVSS.html>)
- Cooray A R and Huterer D, 1999 *Astrophys. J.* **513** L95
- Daly R A, 1994 *Astrophys. J.* **426** 38
- Daly R A and Djorgovski S G, 2003 *Astrophys. J.* **597** 9
- Daly R A and Djorgovski S G, 2004 *Astrophys. J.* **612** 652
- de Bernardis P *et al* , 2000 *Nature* **404** 955
- D’Oderico S, Dessuages-Zavadsky M and Molaro P, 2001 *Astron. Astrophys.* **368** L21
- Fanaroff B L and Riley J M, 1974 *Mon. Not. R. Astron. Soc.* **167** 31P
- Freedman W L *et al* , 2001 *Astrophys. J.* **553** 47
- Gerke B F and Efsthathiou G, 2002 *Mon. Not. R. Astron. Soc.* **335** 33
- Gurvits L I, 1994 *Astrophys. J.* **425** 442
- Guy J, Astier P, Nobili S, Regnault N and Pain R, 2005 *Astron. Astrophys.* **443** 781
- Hanany S *et al* , 2000 *Astrophys. J.* **545** L5
- Hinshaw G *et al* , 2003 *Astrophys. J. Suppl.* **148** 135
- Hinshaw G *et al* , 2006 Preprint astro-ph/0603451
- Huterer D and Turner M S, 1999 *Phys. Rev.* **D60** 081301
- Huterer D and Turner M S, 2001 *Phys. Rev.* **D64** 123527
- Huterer D and Starkman G, 2003 *Phys. Rev. Lett.* **90** 031301
- Hu W and Sugiyama N, 1995 *Phys. Rev.* **D51** 2599
- Jackson J C, 1973 *Mon. Not. R. Astron. Soc.* **162** 11P
- Jackson J C and Dodgson M, 1997 *Mon. Not. R. Astron. Soc.* **285** 806
- Jackson J C, 1998 *Mon. Not. R. Astron. Soc.* **296** 619
- Jackson J C and Dodgson M, 1998 *Mon. Not. R. Astron. Soc.* **297** 923
- Jackson J C, 2004 *JCAP* **11** 7
- Jassal H K, Bagla J S and Padmanabhan T, 2006 Preprint astro-ph/0601389
- Jónnson J, Goobar A, Amanullah R and Bergström L, 2004 *JCAP* **09** 7
- Kellermann K I, 1993 *Nature* **361** 134
- Kirkman D, Tytler D, Suzuki N, O’Meara J and Lubin D, 2003 *Astrophys. J. Suppl.* **149** 1
- Kühr H, Witzel A, Pauliny-Toth I I K and Nauber U, 1981 *Astron. Astrophys.* **45** 367
- Legg T H, 1970 *Nature* **226** 65
- Linder E V, 2003 *Phys. Rev. Lett.* **90** 91031
- Linder E V, 2004 *Phys. Rev.* **D70** 061302
- Masson C R, 1980 *Astrophys. J.* **242** 8
- Maor I, Brustein R and Steinhardt P J, 2001 *Phys. Rev. Lett.* **86** 6
- Maor I, Brustein R, McMahon J and Steinhardt P J, 2002 *Phys. Rev.* **D65** 123003
- Miley G K, 1971 *Mon. Not. R. Astron. Soc.* **152** 477
- Mosoni L, Frey S, Gurvits L I, Garrett M A, Garrington S T and Tsvetanov Z I, 2006 *Astron. Astrophys.* **445** 413
- Mukhanov V, 2004 *Int. J. Theor. Phys.* **43** 623

- Nilsson K, Valtonen J, Kotilainen J and Jaakkola T, 1993 *Astrophys. J.* **413** 453
- Parkes Catalogue, 1990, Australia Telescope National Facility, Wright A and Otrupcek R (Eds)
(<http://www.parkes.atnf.csiro.au/research/surveys/pkscat90.html>)
- Perlmutter S. *et al* , 1997 *Astrophys. J.* **483** 565
- Perlmutter S. *et al* , 1999 *Astrophys. J.* **517** 565
- Pettini M and Bowen D V, 2001 *Astrophys. J.* **560** 41
- Preston R A, Morabito D D, Williams J G, Faulkner J, Jauncey D L, and Nicolson G, 1985 *Astronom. J.* **90** 1599 (P85)
- Ratra B and Peebles P J E, 1988 *Phys. Rev.* **D37** 3406
- Richter G M, 1973 *Astrophys. Lett.* **13** 63
- Riess A G *et al* , 1998 *Astronom. J.* **116** 1009
- Riess A G *et al* , 2004 *Astrophys. J.* **607** 665
- Riess A G, Li W, Stetson P B, Filippenko A V, Jha S, Kirshner R P, Challis P M, Garnavich P M and Chornock R, 2005 *Astrophys. J.* **627** 579
- Schmidt B P *et al* , 1998 *Astrophys. J.* **507** 46
- Seljak U and Zaldarriaga M, 1996 *Astrophys. J.* **469** 437
- Singal A K, 1988 *Mon. Not. R. Astron. Soc.* **233** 87
- Spergel D N *et al* , 2003 *Astrophys. J. Suppl.* **148** 175
- Spergel D N *et al* , 2006 Preprint astro-ph/0603449
- Thompson A R, Moran J M and Swenson G W Jr, 1986 *Interferometry and Synthesis in Radio Astronomy* (New York: Wiley) p 13
- Tonry J L *et al* , 2003 *Astrophys. J.* **594** 1
- Véron-Cetty M-P and Véron P, 1991 *A Catalogue of Quasars and Active Galactic Nuclei* (5th Edition ESO Science Report No. 10)
- Wang Y and Freese K, 2006 *Phys. Lett.* **B632** 449
- Weller J and Albrecht A, 2002 *Phys. Rev.* **D65** 103512
- Wilkinson P N, Polatidis A G, Readhead A C S, Xu W and Pearson T J, 1994 *Astrophys. J.* **432** L87

6. Figures

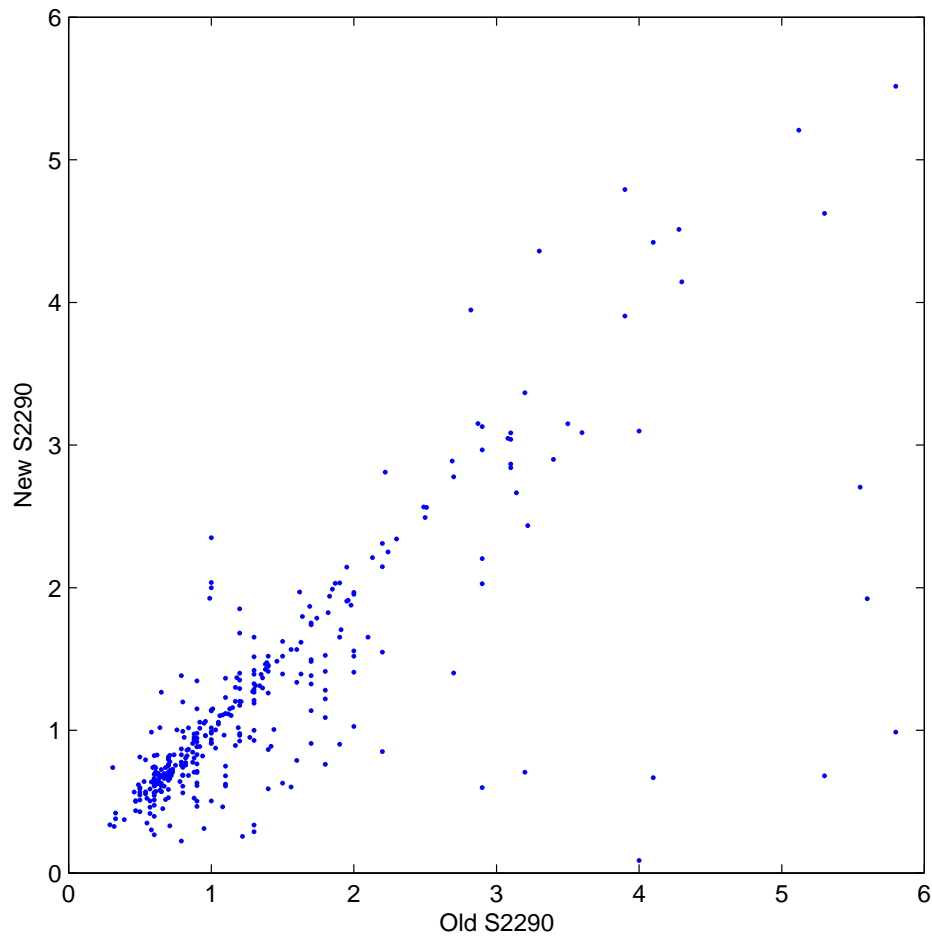


Figure 1. Legacy data. Plot of flux density S2290 derived from the Parkes catalogue PKS90 (New S2290) against the corresponding figure from Preston *et al* (1985) (Old S2290), for those sources (346) which have measures in both. Values of S2290 derived from PKS90 are used in suitable cases when a direct measure is not given in Preston *et al* (1985).

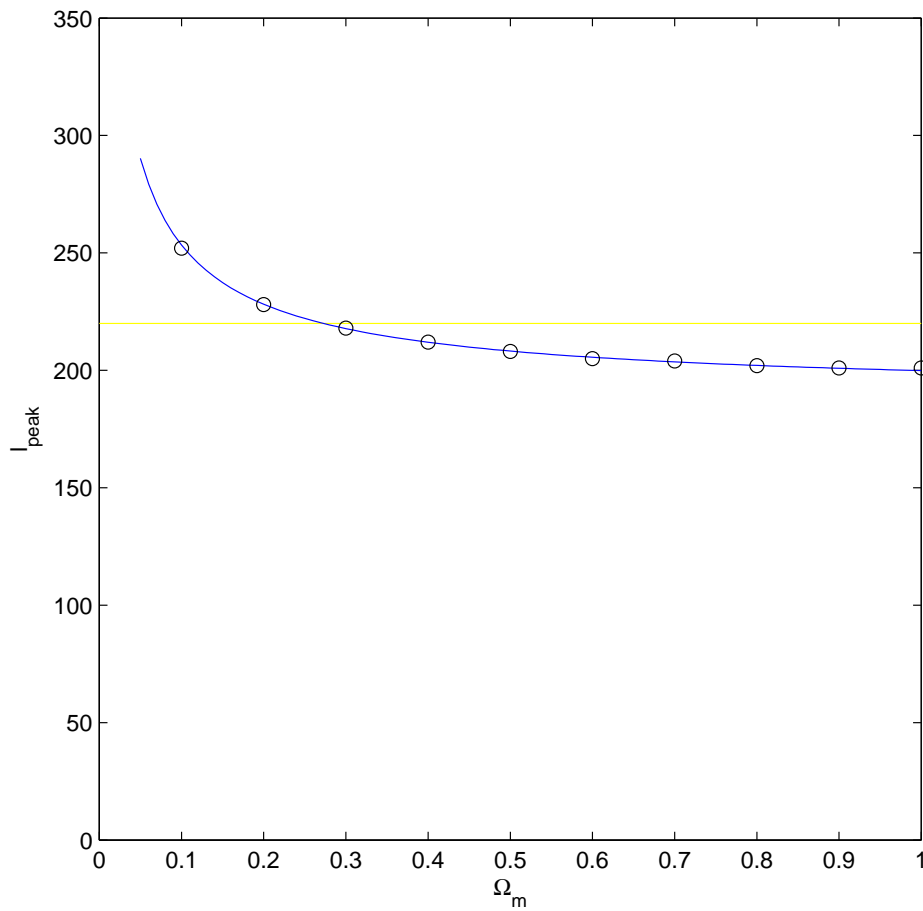


Figure 2. Multipole moment l_{peak} corresponding to the first acoustic peak in the CMB angular spectrum; blue line is the analytical curve according to equations (1), (5) and (6), with $z_r = 1088$, $h = 0.7$ and $\Omega_b = 0.04$; data points are from CMBFAST; all spatially flat: $\Omega_\lambda = 1 - \Omega_m$. The yellow horizontal line is the WMAP figure $l_{\text{peak}} = 220$.

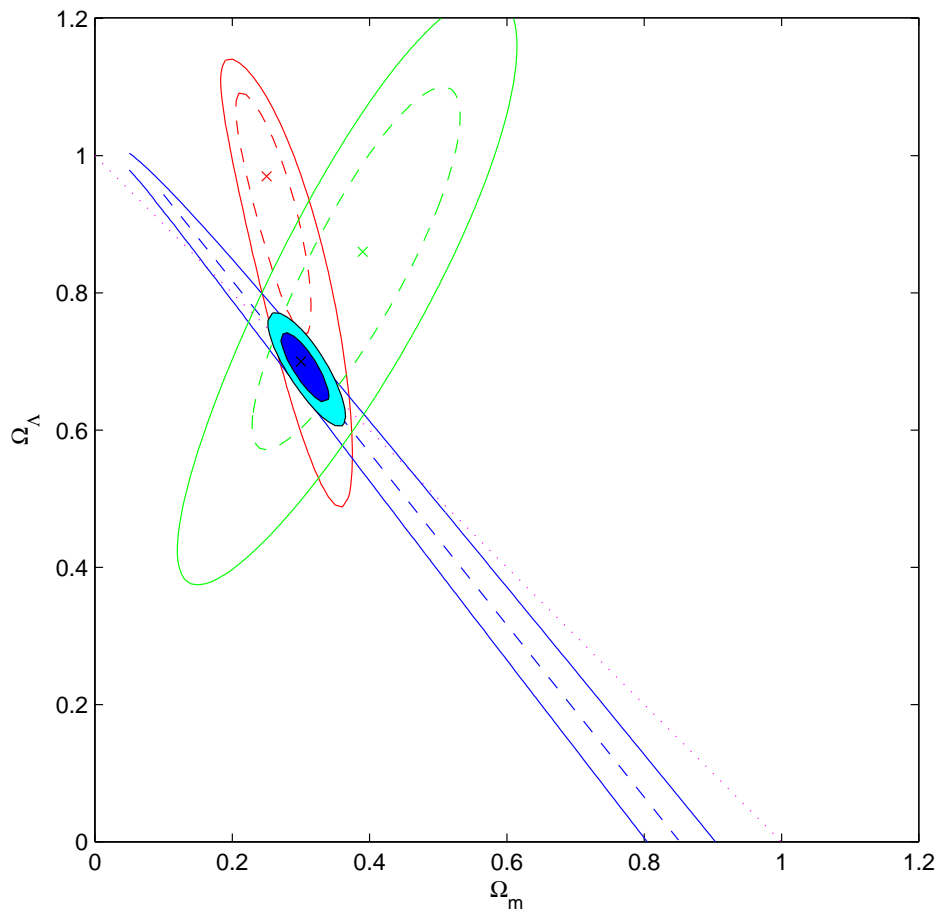


Figure 3. Confidence regions in the Ω_m - Ω_Λ plane, 95% and 68%; red=millisecond radio-sources, blue=acoustic horizon, green=Type Ia supernovae; the filled areas are joint confidence regions for all three; the acoustic horizon fit is exact along the dashed blue line.

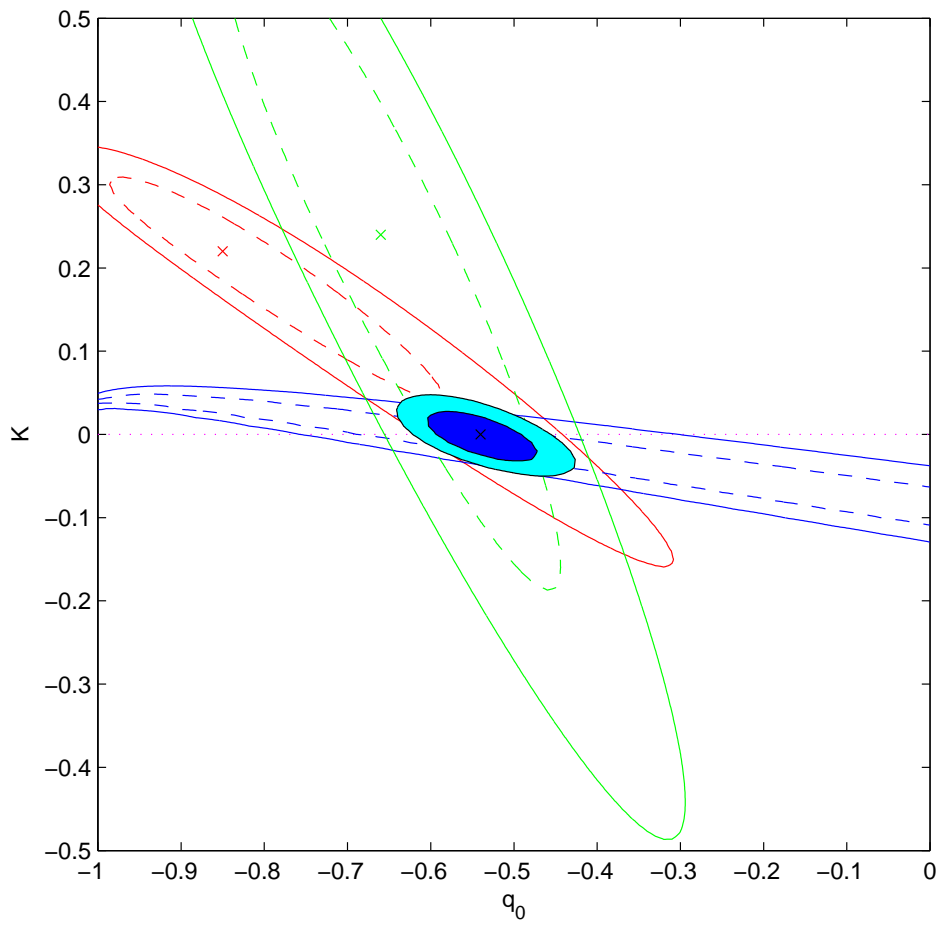


Figure 4. Confidence regions in the q_0 - K plane, 95% and 68%; red=milliarcsecond radio-sources, blue=acoustic horizon, green=Type Ia supernovae; the filled areas are joint confidence regions for all three; the dashed blue lines are now 68% confidence limits.

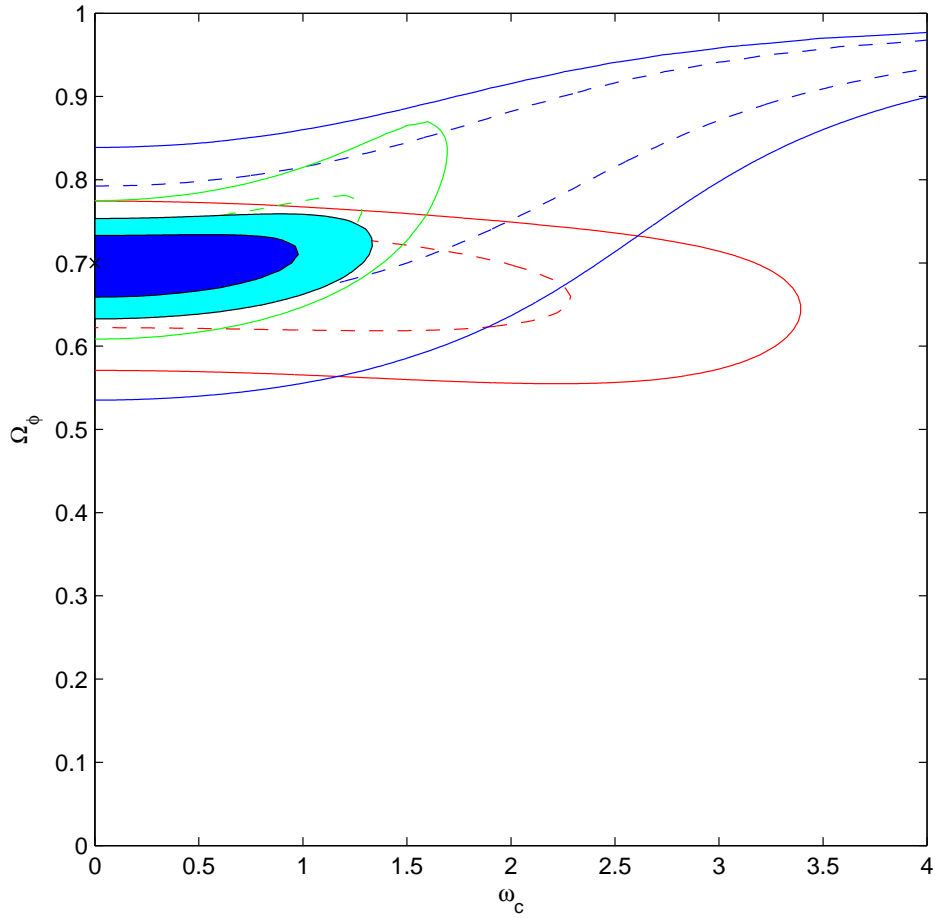


Figure 5. Confidence regions in the ω_C - Ω_ϕ plane, 95% and 68%, where ω_C is Compton frequency in Hubble units; as determined by the three data sets: red=milliarcsecond radio-sources, blue=acoustic horizon, green=Type Ia supernovae; the filled areas are joint confidence regions for all three. Flat universes with evolving scalar vacuum energy governed by a potential $V(\phi) = \omega_C^2 \phi^2/2$.

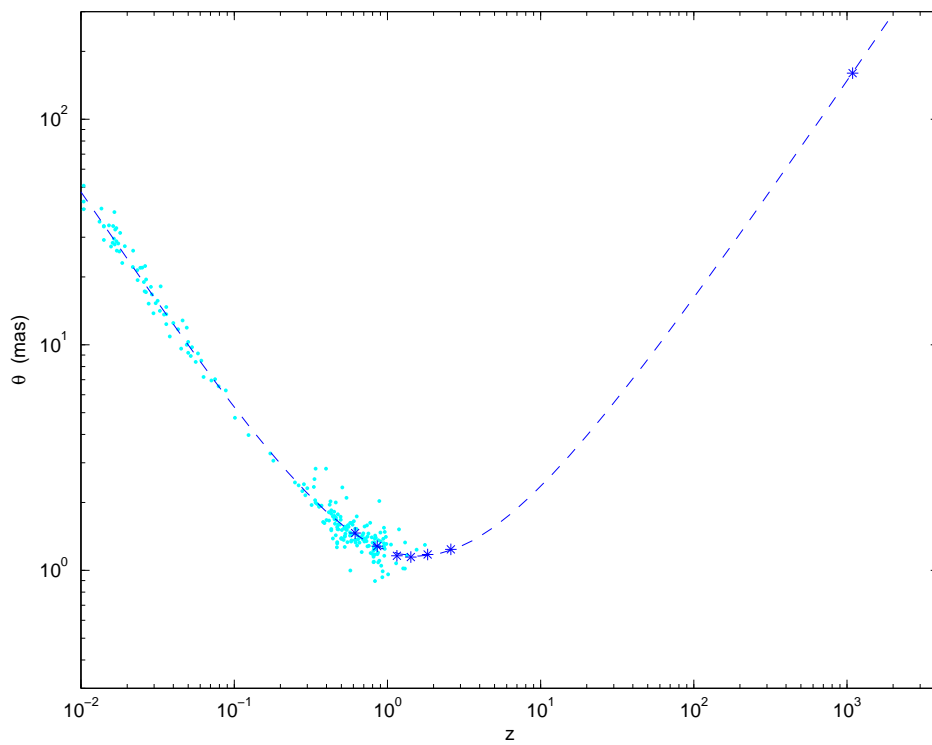


Figure 6. Angular-diameter/redshift diagram; each lower blue star is a bin containing $c. 77$ milliarcsecond radio-sources (see text); the error bars are too small to be seen on this scale, amounting to ± 0.006 in $\log \theta$. Each cyan point corresponds to a supernova transformed into a mock milliarcsecond source. The top blue star represents the acoustic horizon; the error bar is ± 0.0120 in $\log \theta$, corresponding to $h = 0.72 \pm 0.05$.

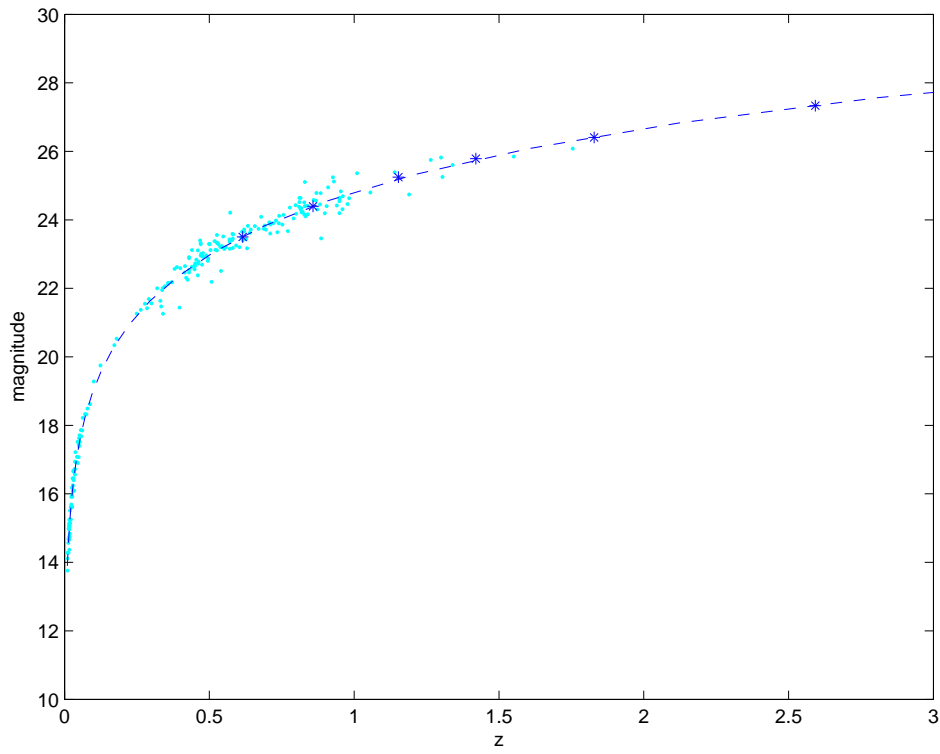


Figure 7. Magnitude/redshift diagram; each cyan point is a supernova. Each blue star represents a bin containing *c.* 77 milliarcsecond radio-sources (see text); the error bars are too small to be seen on this scale, amounting to ± 0.03 magnitudes.